ChemComm

COMMUNICATION

View Article Online
View Journal | View Issue

Cite this: *Chem. Commun.*, 2023, **59**, 482

Received 15th November 2022,
Accepted 8th December 2022

DOI: 10.1039/d2cc06177e

rsc.li/chemcomm

Overlooked potential of *N,N*-bidentate directing-groups in Ni-catalyzed C–H functionalization of benzamides†

Weirong Wu,[a] Xufang Zhao,[c] Guang Chen,[c] Lingjun Liu,[f] Yulin Li,[b] Tao Chen,[b] Tony D. James *[de] and Yuxia Liu *[c]

The Ni-catalyzed reactions of benzamides with bicyclic alkenes were explored using DFT calculations. An unprecedented "N–H deprotonation circumvented" catalytic mechanism was proposed, over the more common N–H/C–H activation mechanism, in which (i) the circumvention of N–H deprotonation ensures the presence of N–H···O hydrogen bond interaction, thereby stabilizing the critical *ortho*-C–H functionalization TS; and (ii) the N–H moiety retention results in a weak N···Ni σ-coordination, which is flexible to the configurational conversion during the key alkene insertion. These overlooked aspects of the functionalized *N,N*-bidentate directing groups will aid the design of new related catalytic reactions.

Transition-metal catalyzed C–H functionalization reactions have proven to be one of the most powerful and promising approaches for the construction of C–C and C–heteroatom bonds due to significant step- and atom-economy.[1] The key challenge in exploring these reactions is how to discriminate multiple C–H bonds present in the reactant molecules. Considerable efforts have been devoted to incorporating directing groups (DGs) into the substrate[2] to achieve site-selective C–H activation,[3] in which, bidentate DGs are vital owning to their enhanced ability to achieve selective *ortho*-C–H functionalization, which is not possible using monodentate DGs.[4] Since the seminal work by Daugulis *et al.*,[5] *N,N*-bidentate DGs have been widely used for C–H functionalization of aromatic amides catalyzed by various transition-metals complexes involving Ni, Co, Ru, Rh, Cu, and Pd.[6] Among these C–H activation protocols, the coupling partners include alkynes, alkenes, and a wide range of halides *etc.*,[7] significantly expanding the applications of these transformations.

Mechanistically, it is generally accepted that this type of reaction involves the programmed cleavages of the N–H and *ortho*-C–H bonds to form a metallacycle species as a key intermediate (Scheme 1A),[8] in which, the N–H cleavage is an indispensable step to direct *ortho*-C–H activation. A series of computational studies have been successively established for these reactions with alkynes,[9] arynes,[10] halides[11] and I_2,[12] where minimal divergence from the commonly accepted mechanism is observed.

Recently, using the 8-aminoquinoline(8-AQ) as a *N,N*-bidentate DG, Chatani *et al.* reported the Ni-catalyzed nonacidic

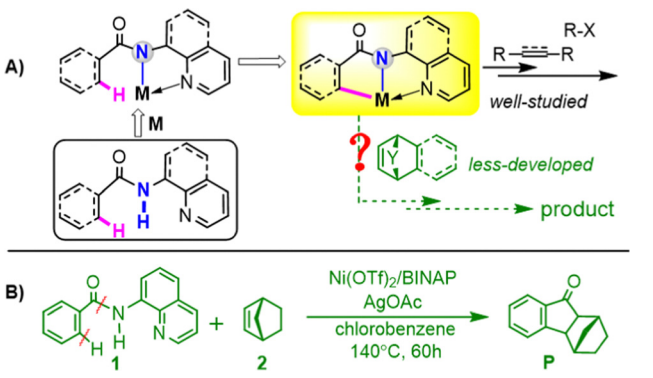

Scheme 1 (A) Commonly reported mechanism for transition-metal catalyzed C–H activation of amides utilizing the *N,N*-bidentate directing group. (B) Ni-catalyzed reaction of *N*-(quinolin-8-yl)benzamide **1** with norbornene **2** reported by Chatani *et al.*[13]

[a] *School of Environment and Chemical Engineering, Chongqing Three Gorges University, Chongqing, China*
[b] *Key Laboratory of Tibetan Medicine Research & Qinghai Key Laboratory of Qinghai-Tibet Plateau Biological Resuorces, Northwest Institute of Plateau Biology, Chinese Academy of Science, Xining 810001, Qinghai, P. R. China*
[c] *Shaanxi Key Laboratory of Chemical Additives for Industry, College of Chemistry and Chemical Engineering, Shaanxi University of Science and Technology, Xi' an 710021, China. E-mail: liuyuxia2008@163.com*
[d] *Department of Chemistry, University of Bath, Bath BA2 7AY, UK. E-mail: chstdj@bath.ac.uk*
[e] *School of Chemistry and Chemical Engineering, Henan Normal University, Xinxiang, 453007, P. R. China*
[f] *School of Chemistry and Chemical Engineering, Qufu Normal University, Qufu, 273165, P. R. China*

† Electronic supplementary information (ESI) available. See DOI: https://doi.org/10.1039/d2cc06177e

C–H functionalization of aromatic amides with bicyclic alkenes[13] to produce 1-indanone derivatives as potential pharmaceuticals for the treatment of Alzheimers,[14] Parkinson's diseases[15] and hepatitis C virus.[16] A representative reaction is given in Scheme 1B, where *N*-(quinolin-8-yl)benzamide **1** and norbornene **2** in chlorobenzene at 140 °C produces the cyclic product **P** in high yield. However, a preliminary DFT examination (see the Computational details in the ESI†) for the reaction in Scheme 1B indicates that the generally accepted N–H/C–H activation mechanism is not operable under the given conditions due to high energy barrier (over 37 kcal mol^{-1} in Fig. 1). Thus, further theoretical explorations are required to unveil the mechanistic puzzle, and specially, the potential of the *N*,*N*-bidentate DG involved, which would be particularly useful for designing related catalytic reactions.

For the representative reaction in Scheme 1B, we first calculated the free-energy profile along the N–H/C–H activation pathway in Fig. 1. The reaction is initiated by the coordination of Ni(OTf)$_2$ with BINAP ligand (denoted as L) to generate the complex **IM1**. Following participation of **1** and AgOAc, the N^1–H deprotonation smoothly occurs *via* the cyclic transition state **TS2-3** with a barrier of only 1.9 kcal mol^{-1}, affording intermediate **IM3**. Upon LAgOAc addition to give **IM4** after releasing LAgOTf and HOAc,[17] a OAc-assisted concerted metalation-deprotonation (CMD) gives nickelacycle species **IM5**.[18,19] Subsequently, the C^4=C^5 bond of **2** inserts into the Ni–C^1 bond forming **IM6**, a seven-membered energy nickelacycle species, which further evolves into product **P**.[20] Note that the elementary step for alkene insertion *via* **TS5-6** has a barrier of 31.7 kcal mol^{-1} relative to **IM5**, which, results in an overall barrier of up to 37.6 kcal mol^{-1} (the difference between **TS5-6** and **IM3**).[9b] Obviously, such a high energy barrier is impossible to accomplish under the given conditions. The main reason could be attributed to the instability of **IM6**, in which a seven-membered nickelacycle is involved. After N^1–H deprotonation, compared with the previous weak Ni–N^1 σ-coordination, a strong N^1–Ni σ-bond forms, which results in a relatively rigid seven-membered nickelacycle in **IM6**. Thus, it is not surprising that a significant energy consumption occurs on formation of **IM6**. In this case, the commonly asserted pathway following a tandem N^1–H deprotonation/C^1–H-cleavage sequence is clearly not operative for the reaction under consideration and as such a more reasonable mechanism is required.

To circumvent the rigid seven-membered nickelacycle during the reaction, based on the theoretical investigation, we tentatively developed a N^1–H deprotonation free mechanism, where an extra N–H···O hydrogen bond interaction is present in the OAc-assisted CMD process, as well as a weak Ni···N coordination in the crucial alkene insertion step. The proposed mechanism is initiated by C^1–H activation. As shown in Fig. 2, from **IM1** in Fig. 1, with the addition of **1** and AgOAc, the OAc-assisted CMD process proceeds to afford the five-membered cyclic complex **IM8**. The C^1–H activated TS, **TS7-8**, includes a N^1–H···O hydrogen bond, with a barrier of 11.8 kcal mol^{-1} relative to **IM1**. After the approach of **2** to **IM8** with L release to give **IM9**,[21] two elementary steps follow: the C^4=C^5 coordination of **2** to the Ni centre (**IM9** → **IM10**) and then C^4=C^5 insertion into the Ni–C^1 bond (**IM10** → **IM11**), leading to the alkene inserted species **IM11**. The transformation from **IM9** to **IM11** is relatively facile with a barrier of 15.6 kcal mol^{-1} (the difference between **TS10-11** and **IM9**).

After alkene insertion, according to Chatani's proposal,[13] the product **P** would be obtained *via* an intramolecular nucleophilic cyclization followed by C^3–N^1 cleavage with the assistance of AgOAc. Our calculated results in Fig. 2 indicate that, from **IM11**, after the ligand exchange between L and HOAc,[22] this intramolecular nucleophilic cyclization takes place *via* **TS12-13**, in which, the (Ni-)OTf moiety is simultaneously transferring to the *trans* position from the *cis* position of the N(H) moiety to keep the planar configuration of the Ni center.[23] This concerted step results in a barrier of 33.0 kcal mol^{-1} and thus is identified as rate-determining. The resultant complex **IM13** then experiences a facile C^3–N^1 cleavage with a barrier of only 2.0 kcal mol^{-1} and gives rise to structure **IM14**, in which **P** has almost formed. Ultimately, **IM14** combines with HOAc and **1** leading to product **P** and active catalyst **IM2**. The simultaneously obtained quinolin-8-amine **3**, as a by-product, is further oxidized by AgOAc into *N*-(quinolin-8-yl)acetamide.[13]

To provide a better understanding on the pathway in Fig. 2, we performed comparative analyses of the transition states for two key steps involved in Fig. 1 and 2: the C^1–H cleavage and alkene insertion, and the calculated results are given in Fig. 3. In the case of the C^1–H cleavage process (left column), **TS7-8** (including the N^1–H···O hydrogen bond) is slightly higher in energy than **TS4-5** (TS after N–H deprotonation) (−13.8 *vs.* −20.2 kcal mol^{-1}). If no-hydrogen-bond is considered, the resultant C^1–H activation TS, denoted as **TS7-8′**, is energetically less favorable by 10.1 kcal mol^{-1} than **TS7-8**. Thus, it is believed that the N–H···O hydrogen bond interaction involved facilitates the stability of **TS7-8**. From the performed noncovalent interaction analyses (NCIs),[24] one can identify in Fig. 3 (left column) that a significant N^1–H···O hydrogen bond interaction (blue isosurface) is present in **TS7-8**, but very weak dispersion interaction (green isosurface) is observed in **TS7-8′**. In general, the N^1–H···O hydrogen bond plays a pivotal role on stabilizing **TS7-8**.

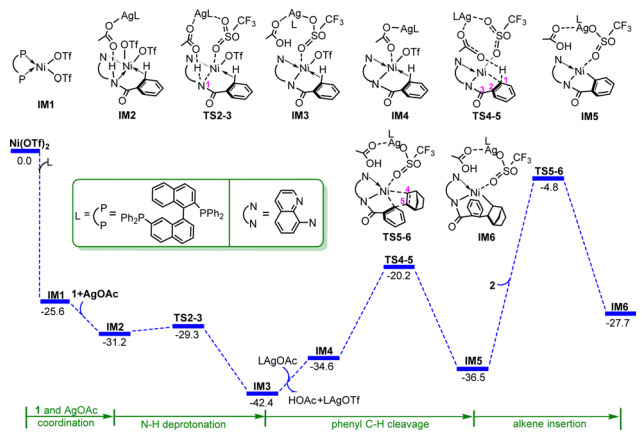

Fig. 1 Gibbs free energy profile in chlorobenzene solvent along the pathway forming the product **P** according to the commonly accepted route. The free energies are given in kcal mol^{-1}.

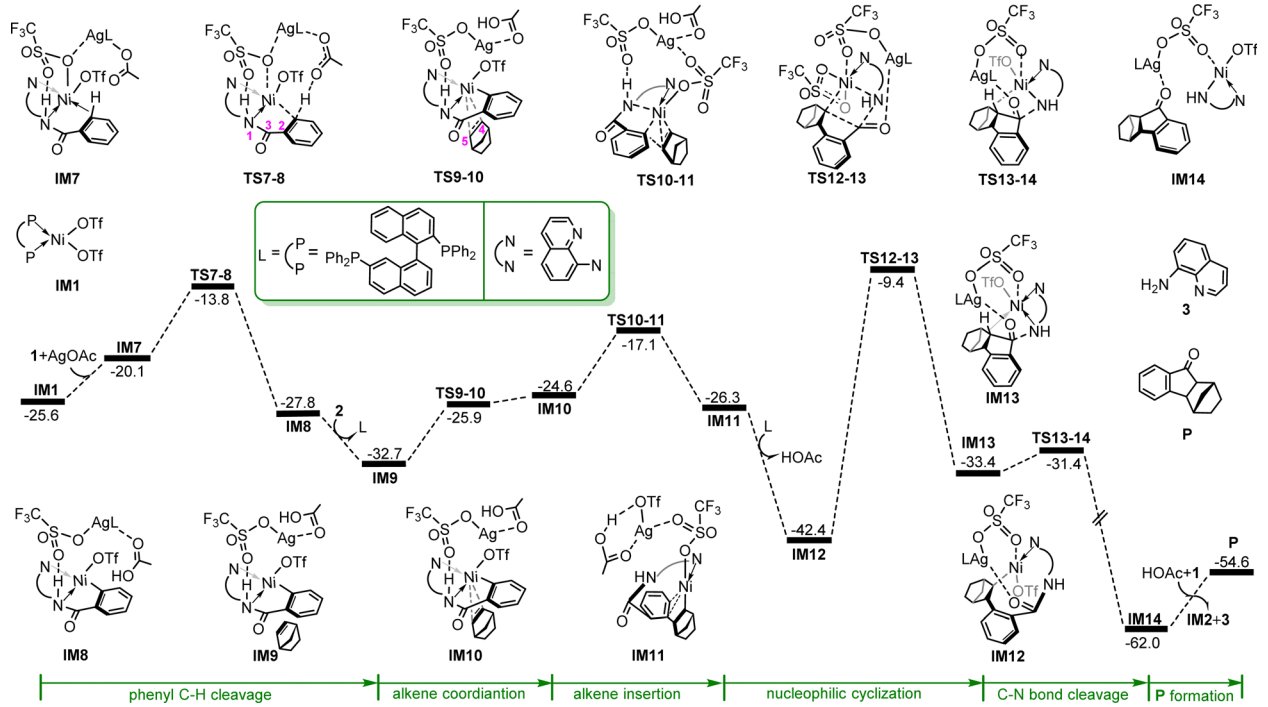

Fig. 2 Gibbs free energy profiles in chlorobenzene solvent for **P** formation established in the present work. The free energies are given in kcal mol^{-1}.

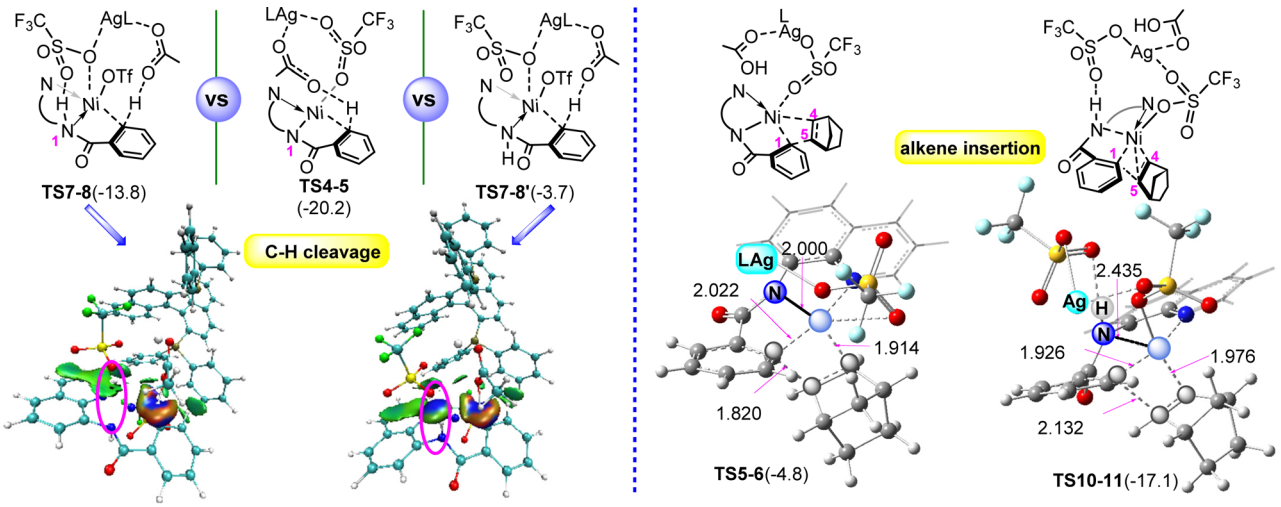

Fig. 3 Noncovalent interaction analyses for the C–H cleavage TSs, **TS7-8**, **TS4-5**, **TS7-8′** (left column, isosurface value = 0.01) as well as the geometries of two alkene insertion TSs, **TS5-6** (HOAc is not shown for clarity) and **TS10-11** (right column). The free energies are given in kcal mol^{-1}.

Next, we turned our attention to the alkene insertion step TSs (Fig. 3, right column). **TS10-11** is found to have appreciably lower free energy than **TS5-6**, −17.1 *vs.* −4.8 kcal mol^{-1}, which was supported by the calculated bond distances. In **TS10-11**, the Ni···C^1 (1.926 Å) is much shorter than 2.022 Å in **TS5-6**, while the Ni···C^4 and Ni···C^5 (1.976 and 2.132 Å) are longer than the corresponding distances (1.914 and 1.820 Å) in **TS5-6**. Obviously, **TS10-11** is easier to surmount than **TS5-6**. The origin might be derived from the discrepancy in the Ni–N^1 interaction modes involved. It is noted that **TS10-11** features weak Ni–N^1 σ-coordination, which is flexible to adapt the configurational transformation resulting from the alkene insertion. In sharp contrast, the Ni–N^1 σ-bond is included in **TS5-6**. Such a rigid bond brings about a large structural distortion and thus results in a significant energy penalty for **TS5-6**. Obviously, the N^1–H retention, due to the lack of N^1–H deprotonation, is intrinsically essential for facilitating the alkene insertion.

In summary, the detailed mechanisms for the Ni-catalyzed reaction of *N*-(quinolin-8-yl)benzamide **1** with norbornene **2** have been computationally evaluated. The commonly reported

N–H/C–H activation mechanism was found to be kinetically inaccessible under the given conditions due to the high energy requirement. In this work, a unique ''N–H deprotonation circumvented'' catalytic mechanism is proposed, which highlights two properties of the *N*,*N*-bidentate group: (i) absence of N–H deprotonation leading to N–H···O hydrogen bond interaction, (ii) the N–H moiety retention resulting in N···Ni weak σ-coordination. It was found that the N–H···O hydrogen bond interaction facilitates the critical *ortho*-C–H functionalization, and N···Ni σ-coordination contributes significantly to the key alkene insertion, facilitating the reaction. These aspects have previously been overlooked, however we expect they may be important for other relevant catalytic reactions.

This work was jointly supported by the National Natural Science Foundation of China (No. 22174090), the Natural Science Foundation of Shaanxi Province (2022JM-089), Key Laboratory of Emergency and Trauma (Hainan Medical University), Ministry of Education (KLET-201903). TDJ wishes to thank the Royal Society for a Wolfson Research Merit Award and the Open Research Fund of the School of Chemistry and Chemical Engineering, Henan Normal University for support (2020ZD01).

Conflicts of interest

There are no conflicts to declare.

References

1 (*a*) M. Albrecht, *Chem. Rev.*, 2010, **110**, 576; (*b*) T. Brückl, R. D. Baxter, Y. Ishihara and P. S. Baran, *Acc. Chem. Res.*, 2012, **45**, 826.
2 S. R. Neufeldt and M. S. Sanford, *Acc. Chem. Res.*, 2012, **45**, 936.
3 (*a*) L. Ackermann, *Chem. Rev.*, 2011, **111**, 1315; (*b*) C. S. Yeung and V. M. Dong, *Chem. Rev.*, 2011, **111**, 1215; (*c*) K. M. Engle, T. S. Mei, M. Wasa and J.-Q. Yu, *Acc. Chem. Res.*, 2012, **45**, 788.
4 G. Rouquet and N. Chatani, *Angew. Chem., Int. Ed.*, 2013, **52**, 11726.
5 (*a*) V. G. Zaitsev, D. Shabashov and O. Daugulis, *J. Am. Chem. Soc.*, 2005, **127**, 13154; (*b*) E. T. Nadres, G. I. F. Santos, D. Shabashov and O. Daugulis, *J. Org. Chem.*, 2013, **78**, 9689.
6 (*a*) G. Rouquet and N. Chatani, *Angew. Chem., Int. Ed.*, 2013, **52**, 11726; (*b*) R. He, Z.-T. Huang, Q.-Y. Zheng and C. Wang, *Tetrahedron Lett.*, 2014, **55**, 5705; (*c*) M. S. Khan, A. Haque, M. K. Al-Suti and P. R. Raithby, *J. Organomet. Chem.*, 2015, **793**, 114; (*d*) X. Yang, G. Shan, L. Wang and Y. Rao, *Tetrahedron Lett.*, 2016, **57**, 819.
7 (*a*) X.-F. Yang, X.-H. Hu and T.-P. Loh, *Org. Lett.*, 2015, **17**, 1481; (*b*) P. Gandeepan, P. Rajamalli and C.-H. Cheng, *Angew. Chem., Int. Ed.*, 2016, **55**, 4308; (*c*) Z. He and Y. Huang, *ACS Catal.*, 2016, **6**, 7814; (*d*) B. Khan, R. Kant and D. Koley, *Adv. Synth. Catal.*, 2016, **358**, 2352; (*e*) T. Uemura, M. Yamaguchi and N. Chatani, *Angew. Chem., Int. Ed.*, 2016, **55**, 3162; (*f*) Y. Aihara and N. Chatani, *ACS Catal.*, 2016, **6**, 4323; (*g*) Q. Zheng, C. Liu, J. Chen and G. Rao, *Adv. Synth. Catal.*, 2020, **362**, 1406.
8 (*a*) Y. Dang, X. Deng, J. Guo, C. Song, W. Hu and Z.-X. Wang, *J. Am. Chem. Soc.*, 2016, **138**, 2712; (*b*) D. L. Davies, S. A. Macgregor and C. L. McMullin, *Chem. Rev.*, 2017, **117**, 8649; (*c*) Y. Liu, K. Wang, B. Ling, G. Chen, Y. Li, L. Liu and S. Bi, *Catal. Sci. Technol.*, 2020, **10**, 4219; (*d*) Y.-F. Yang, G.-J. Cheng, P. Liu, D. Leow, T.-Y. Sun, P. Chen, X. Zhang, J.-Q. Yu, Y.-D. Wu and K. N. Houk, *J. Am. Chem. Soc.*, 2014, **136**, 344.
9 (*a*) S. R. Neufeldt, G. Jiménez-Osés, J. R. Huckins, O. R. Thiel and K. N. Houk, *J. Am. Chem. Soc.*, 2015, **137**, 9843; (*b*) K. Yamazaki, A. Obata, A. Sasagawa, Y. Ano and N. Chatani, *Organometallics*, 2019, **38**, 248; (*c*) H. M. Omer and P. Liu, *ACS Omega*, 2019, **4**, 5209.
10 C. Chen, Y. Hao, T.-Y. Zhang, J.-L. Pan, J. Ding, H.-Y. Xiang, M. Wang, T.-M. Ding, A. Duan and S.-Y. Zhang, *Chem. Commun.*, 2019, **55**, 755.
11 (*a*) L. Huang, Q. Li, C. Wang and C. Qi, *J. Org. Chem.*, 2013, **78**, 3030; (*b*) A. L. Dewyer and P. M. Zimmerman, *ACS Catal.*, 2017, **7**, 5466.
12 B. E. Haines, J.-Q. Yu and D. G. Musaev, *Chem. Sci.*, 2018, **9**, 1144.
13 A. Skhiri and N. Chatani, *Org. Lett.*, 2019, **21**, 1774.
14 L. Huang, H. Miao, Y. Sun, F. Meng and X. Li, *Eur. J. Med. Chem.*, 2014, **87**, 429.
15 A. Affini, S. Hagenow, A. Zivkovic, J. Marco-Contelles and H. Stark, *Eur. J. Med. Chem.*, 2018, **148**, 487.
16 L. Chan, O. Pereira, T. J. Reddy, S. K. Das, C. Poisson, M. Courchesne, M. Proulx, A. Siddiqui, C. G. Yannopoulos, N. Nguyen-Ba, C. Roy, D. Nasturica, C. Moinet, R. Bethell, M. Hamel, L. L'Heureux, M. David, O. Nicolas, P. Courtemanche-Asselin, S. Brunette, D. Bilimoria and J. Bédard, *Bioorg. Med. Chem. Lett.*, 2004, **14**, 797.
17 From **IM3**, the C–H cleavage followed by alkene insertion pathway is found to be less preferred than the one from **IM4**. Please see Fig. S1 for the details.
18 The possible C–H oxidative additions from **IM5** are also further considered. However, it is found that the resultant **IM17** (Ni^{III} intermediate) and **IM18** (Ni^{IV} species) are even higher in energy than the alkene insertion transition state **TS5-6**. Therefore, the pathways leading to the nickel species with high oxidation state are not operative in the reaction under consideration. Please see Fig. S1 for the details.
19 (*a*) Y. B. Dudkina, R. R. Fayzullin, K. A. Lyssenko, A. T. Gubaidullin, K. V. Kholin, A. I. Levitskaya, M. Yu. Balakina and Y. H. Budnikova, *Organometallics*, 2019, **38**, 1254; (*b*) S.-K. Zhang, R. C. Samanta, A. D. Vecchio and L. Ackermann, *Chem. – Eur. J.*, 2020, **26**, 10936; (*c*) Y. H. Budnikova, *Chem. Rec.*, 2021, **21**, 2148.
20 The alkene insertion step *via* **TS5-6** is believed to be unachievable due to a high energy demand, and therefore, further calculations after **IM6** were not performed.
21 As compared to the L-involved case, the barrier for the no-L-involved alkene insertion process from **IM8** is easier to overcome. Please see Fig. S3 for the details.
22 Other possible nucleophilic cyclization pathways are collected in Fig. S3. It is found that these potential energy profiles are significantly higher than that starting from **IM11**.
23 A diagram of the key bond length scans for **TS12-13** along the IRC pathway is displayed in Fig. S4, which supports the concerted nucleophilic cyclization and the (Ni-)OTf migration.
24 (*a*) T. Lu and F. Chen, *J. Comput. Chem.*, 2012, **33**, 580; (*b*) S. Manzetti and T. Lu, *J. Phys. Org. Chem.*, 2013, **26**, 473.